ARTICLE

A cryogel solar vapor generator with rapid water replenishment and high intermediate water content for seawater desalination

Received 00th January 20xx,
Accepted 00th January 20xx

DOI: 10.1039/x0xx00000x

Shudi Mao,[a] Casey Onggowarsito,[a] An Feng,[a] Stella Zhang,[a] Qiang Fu,*[a] and Long D. Nghiem[a]

Hydrogel-based solar vapor generator (SVG) system, without any additional energy input, is a promising alternative to current energy intensive desalination technologies. Thermal and water managements govern the performance of SVG systems. However, considerable efforts have been devoted to improving thermal management to achieve high evaporation rate, while the research on the water management of the hydrogels is still in its early stages, hindering the development of advanced SVGs. Through systematic selection of polymer precursors with proper glass transition temperature (T_g), here we developed a novel cryogel SVG system with desired properties for water management, such as interconnected pores, rapid-water-replenishment, high intermediate water ratio *etc*. As a result, the resultant cryogels exhibit high intermediate water content of 67%, low equivalent evaporation enthalpy of 861.5 J g^{-1}, excellent evaporation rate of 3.59 kg m^{-1} h^{-1} under one sun, high salt resistance and long-term durability in desalination, showing great potential for practical applications.

Introduction

Water scarcity is a serious issue faced by all human beings.[1] One of the most effective methods to alleviate this issue is to extract freshwater from the ocean or other abundant salty water resources.[2-5] However, the majority of the desalination technologies in commercial use are energy intensive [3, 6, 7] or require significant investment, and ongoing operations and maintenance expenses.[8] Solar vapor generation (SVG) technology has recently emerged as a potential alternative to conventional desalination technologies as it can harvest solar energy and lower the latent evaporation enthalpy to efficiently evaporate water, and then condense the vapor to produce freshwater.[9-11]

SVG performance is regulated by thermal and water management.[12-14] Significant efforts have been made to further improve the thermal management, including by developing advanced photothermal materials [15-17] to improve photo-thermal conversion, constructing rough surfaces to reduce light reflection,[18-20] and optimizing heat insulation to reduce heat loss.[21-28] However, with enhanced thermal management alone, the SVG evaporation rate is limited to the maximum theoretical value of 1.59 kg m^{-2} h^{-1} even at solar radiation of 1 kW m^{-2}.[29, 30] Water management, or the balance between evaporation and the supply of liquid water, is also critical and has to date been mostly neglected. Well-designed water management can reduce evaporation enthalpy by increasing the ratio of intermediate water to free water.[27, 31-34]

One strategy to improve water replenishment is to use the direction freezing method [35, 36] or 3D printing technique [37] to construct vertically aligned channels within the hydrogels. However, these fabrication methods are cumbersome or time-consuming, hindering the large-scale fabrication and application of these SVG systems. Since the hydrogels hydrophilic matrix can trigger particular water states, and induce the generation of intermediate water (with weakened water-polymer bonds) that can escape more readily from the neighboring molecules than the other types of water (*i.e.* free water or bonded water). Thus, another applied strategy is to promote the generation of more intermediate water in the hydrogel SVG to lower the overall water evaporation enthalpy.[27, 31-34] As a result, the advent of a novel hydrogel-based platform with special water management strategies has brought the material design of SVG to a new level, enabling evaporation rates beyond the aforementioned limit.[32, 38]

Cryogel (also known as cryotropic hydrogel) is a macroporous material of significant scientific and engineering value.[39-44] Compared with conventional hydrogels, cryogels exhibit much higher water uptake rate due to interconnected pores and enhanced mechanical robustness due to the 'thicker' walls. Through judicious selection of monomers, we saw this is an opportunity to develop a novel cryogel SVG system by a facile approach to improve water replenishment and intermediate water content at the same time.

Herein, we report the development of a novel cryogel SVG for energy-saving desalination applications. The functional monomers 2-hydroxyethyl acrylate (HEA), and poly(ethylene glycol) diacrylate (PEGDA) were first employed to synthesize cross-linked hydrogels. Due to their low glass transition temperatures (T_gs), we then prepared PHEA- or PPEG-based cryogels by freezing hydrogels at -18 °C and thawing them. As expected, the resultant cryogel SVGs have rapid water replenishment and high intermediate water content at the same time, and hence managed to achieve low evaporation enthalpy (861.5 kJ Kg^{-1}) and high water evaporation rate of 3.59 kg m^{-1} h^{-1} under one

[a] *Centre for Technology in Water and Wastewater (CTWW), School of Civil and Environmental Engineering, University of Technology Sydney, Ultimo, 2007, Australia*
**Corresponding to Qiang Fu, Email: qiang.fu@uts.edu.au*
Electronic Supplementary Information (ESI) available: [details of any supplementary information available should be included here]. See DOI: 10.1039/x0xx00000x

Please do not adjust margins

sun. Furthermore, such SVGs also exhibit high durability, high salt resistance and excellent desalination competence in real seawater desalination, making them prospective for future practical applications.

Results and discussion

In this study, PHEA and PPEG-based cryogels were prepared and evaluated against a conventional PVA hydrogel in the same freeze-thaw process for comparison (Figure 1a). Specifically, three vials were charged with PVA and GA (conventional hydrogel), HEA and MBI (PHEA-based cryogel), and PEGDA (PPEG-based cryogel) in DI water (Figure 1). These vials were denoted as solutions I, II and III, respectively. Then, the same amount graphene oxide (GO) dispersion (as photothermal materials) was added into above solutions, followed by 5 min sonication. Thereafter, the catalyst (HCl) or initiators (APS/TEMED) were added to the solutions I, or II and III, respectively and the mixtures were left steady for 5 min to afford gels (Figure 1). The chemical structures of the precursors and the reaction schemes were illustrated in Figures 1b-1d. Then, these gels were placed in a freezer at -18 °C overnight, thawed in DI water at room temperature, and freeze-dried overnight for characterization and water evaporation tests. We prepared a series of gel SVGs with different solid contents, such as 5 or 10 wt%. The resulting SVGs are denoted as P-GO-x, where P represents PHEA, PPEG or PVA and x represents the corresponding solid contents in the gel.

The glass transition temperatures (T_gs) of the PHEA and PPEG chains are *ca.* -30 °C [45] and -60 °C [46, 47], respectively (< -18 °C), while the T_g of PVA is *ca.* 60 °C [48]). Therefore, the PPEG and PHEA chains are in a rubbery state and can maintain good mobility (i.e. flexible) during the freezing process, while PVA chains are in a crystalline state.[49] As a result, the ice crystals in the PPEG and PHEA gels can grow bigger and bigger until their polymer chains huddle together (Figure 2b-I and II), leading to the formation of thick walls and interconnected macropores after thawing (Figure 2b-III). In contrast, the rigidity of PVA chains is due to their relatively high T_g. We, thus, obtained a conventional PVA hydrogel with smaller pore size (Figure 2a-III).

The successful synthesis of the hydrogels and cryogels is first evidenced by the SEM images of the samples. Figures 2c-2h and Figure S1 show the cross-section SEM images of all three gels. We found that all the gels are porous with abundant and generally uniform internal channels, which can provide pathways for water transport. As

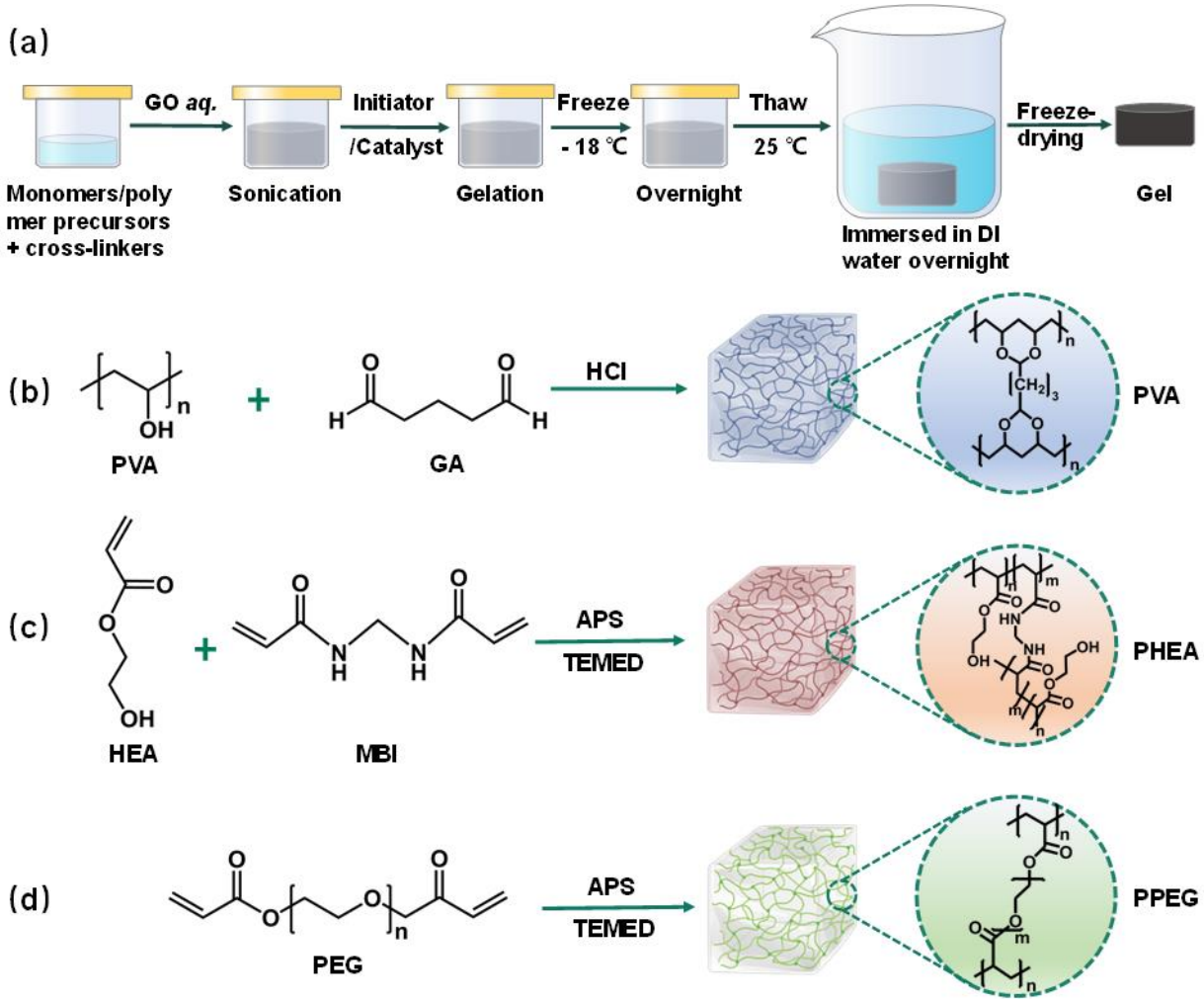

Figure 1. (a) Schematic of the preparation process of the gels and the schematic of chemical structures of all the components during the gelation of (b) PVA gels, (c) PHEA gels, and (d) PPEG gels.

This journal is © The Royal Society of Chemistry 20xx

Please do not adjust margins

ARTICLE

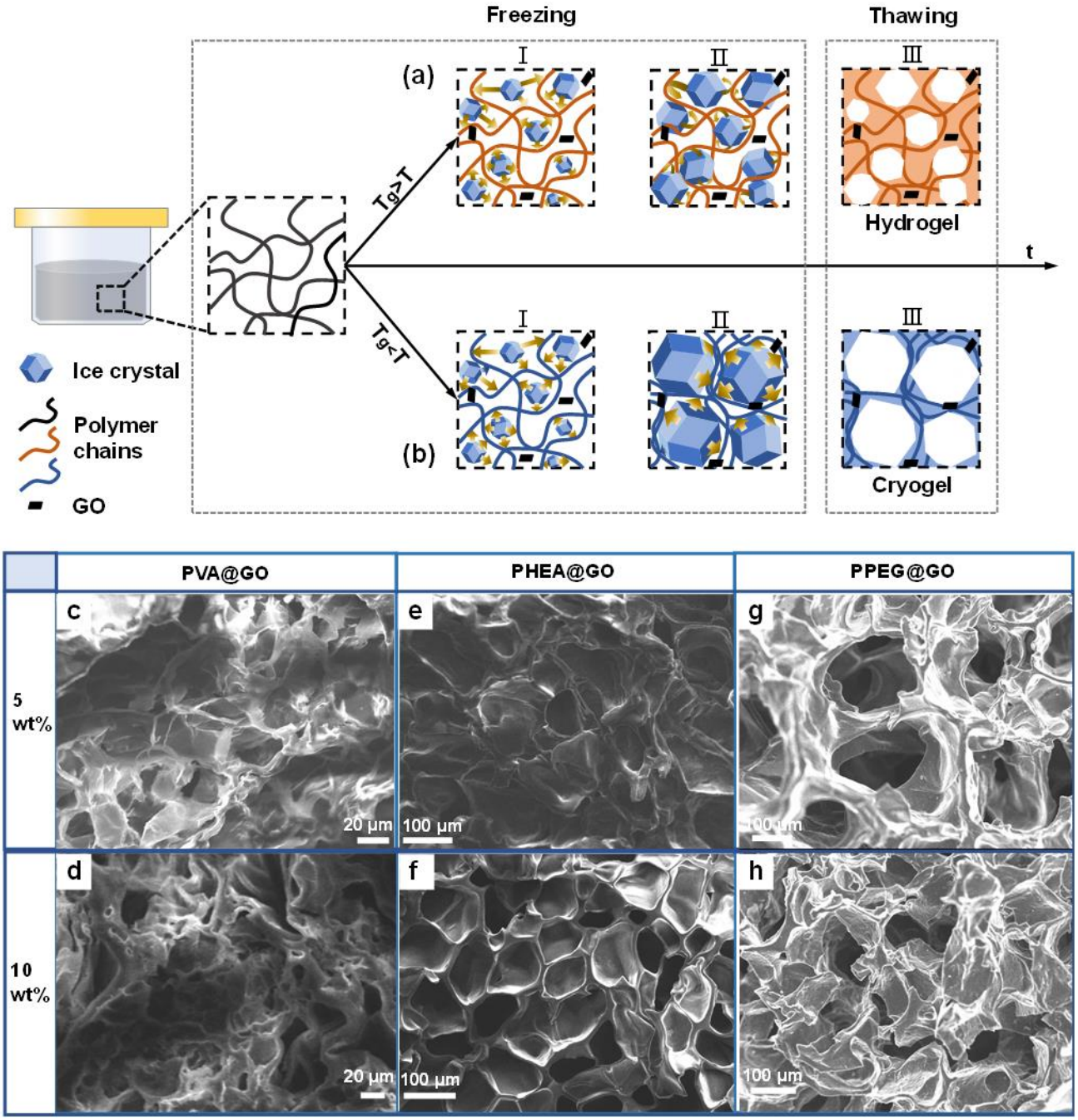

Figure 2. Schematic diagram of the formation process of the (a) hydrogel and (b) cryogels. During the freezing process, (I) the ice crystals firstly generated and then (II) grew bigger with or without limitation of the polymer chains. (III) After thawing, the final gels with pores were obtained. Cross-section SEM images of (c) PVA-GO-5, (d) PVA-GO-10, (e) PHEA-GO-5, (f) PHEA-GO-10, (g) PPEG-GO-5, and (h) PPEG-GO-10 gels from a top-view.

a result of the differences in T_g, PVA hydrogels have relatively smaller internal pores (~5-20 μm) compared with PHEA- (~90-110 μm) and PPEG-based cryogels (~70-130 μm) (Table S1). This result is in good agreement with the pore size properties of hydrogels [32, 50, 51] and cryogels [52-54] reported in previous literature. Increasing the solid content of the polymer network usually leads to enhanced mechanical properties.[44] In this study, P-GO-10 samples always have smaller pores and thicker walls than that of the P-GO-5 samples (Table S1),

Please do not adjust margins

as the P-GO-10 gels have double the solid content to form the matrix. To further confirm the freezing temperature's effect on the pore size, we also synthesized a counterpart of PPEG-GO-10 by freezing it with liquid nitrogen (-197 °C), and denoted it as PPEG-GO-10-LN. As expected, it has a much smaller average pore size of ca. 9.5 μm (Figure S2a and Table S1).

Fourier-Transform infrared (FT-IR) spectra of the PVA-GO-10, PHEA-GO-10 and PPEG-GO-10 were performed to confirm the chemical composition of the fabricated SVGs (Figure 3a). For PVA-based hydrogel SVG, we observed a characteristic absorption signal at 1,100 cm^{-1}, which can be attributed to the stretching vibrations of the secondary hydroxyl group (-CH-OH). In contrast, we observed the vibration peak of the primary hydroxyl (-CH_2-OH) at 1,050 cm^{-1} in the spectrum of PHEA-based cryogel. We also observed the peak at 1,724 cm^{-1}, which can be attributed to the vibration of carbonyl group (C=O) of PHEA or PPEG. What's more, owing to the cross-linker MBI used in the synthesis of PHEA cryogel, we observed the vibration peak of N-H at 1,650 cm^{-1}. At 1,102 cm^{-1} we found the characteristic peak of ester groups (C-O-C) of PPEG. In addition, we also found a signal at 944 cm^{-1}, which is attributed to the unreacted C=C groups of the PEGDA. Overall, these results demonstrate the successful preparation of PVA-, PHEA- and PPEG-based gels, and we can clearly distinguish these three polymer gels with different chemical structures based on their FT-IR spectra.

We then determine their solar absorption using a UV-vis-NIR spectrophotometer. As can be seen in Figure 3b, all SVG gels containing trace amounts of GO as photothermal materials (*ca.* < 2wt% of the xerogel weight) show a broad light absorption range over the entire solar spectrum (from 300 to 2,500 nm).

Compared with a conventional hydrogel, rapid water transport competence is a distinctive and representative feature of cryogel SVGs due to their interconnected macroporous structure. To investigate the difference in water uptake rate among the three SVGs, we recorded the amount of water absorbed by the corresponding dried gels over time (m_t) when immersed in deionized water. The water

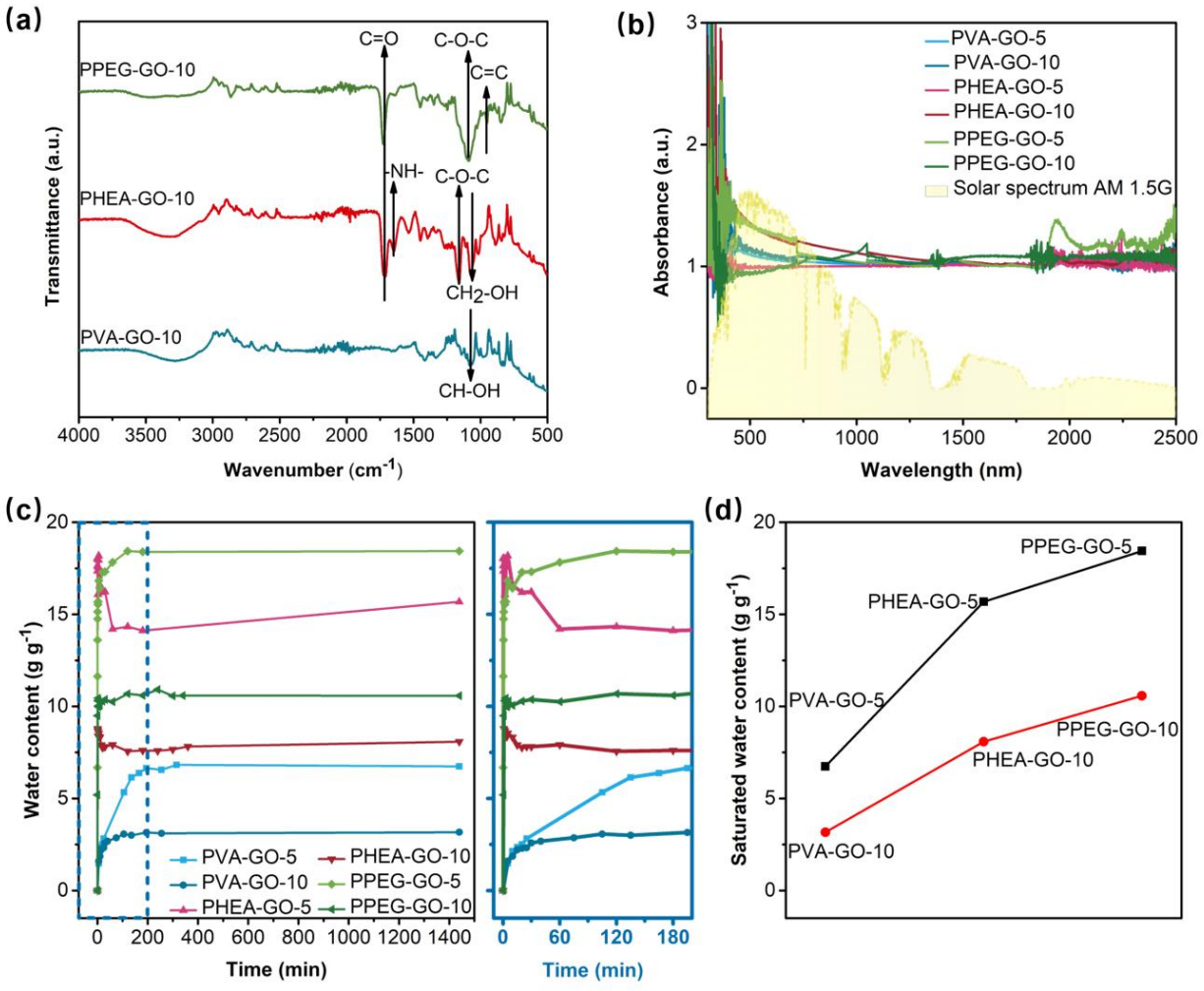

Figure 3. (a) FT-IR spectra of the PVA-GO-10, PHEA-GO-10, and PPEG-GO-10 gels showing their chemical composition. (b) UV-vis-NIR spectra of the gels and the solar spectrum of air mass 1.5 global (AM 1.5 G) with normalised spectral solar irradiance density (the grey area) over the wavelength of 300-2,500 nm. (c) The water content of the gel per gram of the corresponding dry gel plotted against water absorption time (the right figure represents for the first 200 minutes of water absorption). (d) The saturated water content in the well-saturated gel per gram of the corresponding xerogel

This journal is © The Royal Society of Chemistry 20xx

Please do not adjust margins

content is calculated using equation (1):

$$\boldsymbol{Q = m_t/m_{dry}} \quad \text{Eq (1)}$$

where m_{dry} is the mass of the corresponding dried gel. Figure 3c visually shows the capacity for absorbing water of hydrogels and cryogels. The dry PVA hydrogel SVGs can fast absorb water at the initial stage (<20 min), and then the water uptake rate decreased. After 200 minutes, the water content of PVA-GO-10 and PVA-GO-5 reached a plateau (*aka*. saturated state) of 3.17 and 6.74 g g^{-1}, respectively. In sharp contrast, we found the cryogel SVGs' weights *vs*. time curves are nearly vertical at first, suggesting they are almost full of water in less than a minute of contact with water. Their water contents fluctuated slightly over time. As shown in Figure 3d, with the same polymer contents, PPEG-based SVGs have the highest saturated water content of 18.44 and 10.58 g g^{-1} for PPEG-GO-5 and PPEG-GO-10, respectively. While the PHEA cryogels display a saturated water content of 15.68 and 8.08 g g^{-1} for PHEA-GO-5 and PHEA-GO-10, respectively. All these values are higher than that of PVA hydrogel SVGs. Interestingly, when we doubled the polymer (solid) content of the gels, their saturated water content decreased by *ca*. 50%. This can be attributed to the smaller pores and 'thicker' walls in gels with higher polymer content. Notably, the rapid frozen PPEG-GO-10-LN sample showed a gradual water absorption, much slower than that of PPEG-GO-10 cryogel (Figure S2b). The slow water absorption speed and small pore size can further validate the synthesis of a conventional evaporator by freezing them below their T_gs.

Increasing intermediate water content in a SVG system is an effective water management strategy to boost evaporation rate. Raman measurements of all gel samples (containing water) were conducted and their intermediate water contents were determined via peak fitting (Figures 4a-4f). The pink peaks at 3,233 cm^{-1} and 3,401 cm^{-1} represent for the free water with four hydrogen bonds, while the light blue peaks around 3,514 cm^{-1} and 3,630 cm^{-1} represent for the intermediate water with weaken hydrogen bonds.[32, 51] The calculated molar ratio of intermediate water (IW): the sum of intermediate water and free water (IW+FW) in PVA-GO-5, PHEA-GO-5 and PPEG-GO-5 were 0.336:1, 0.511:1 and 0.613:1, respectively. Intriguingly, although the P-GO-5 samples possess larger pore sizes and higher water absorption capacity, the P-GO-10 samples display higher

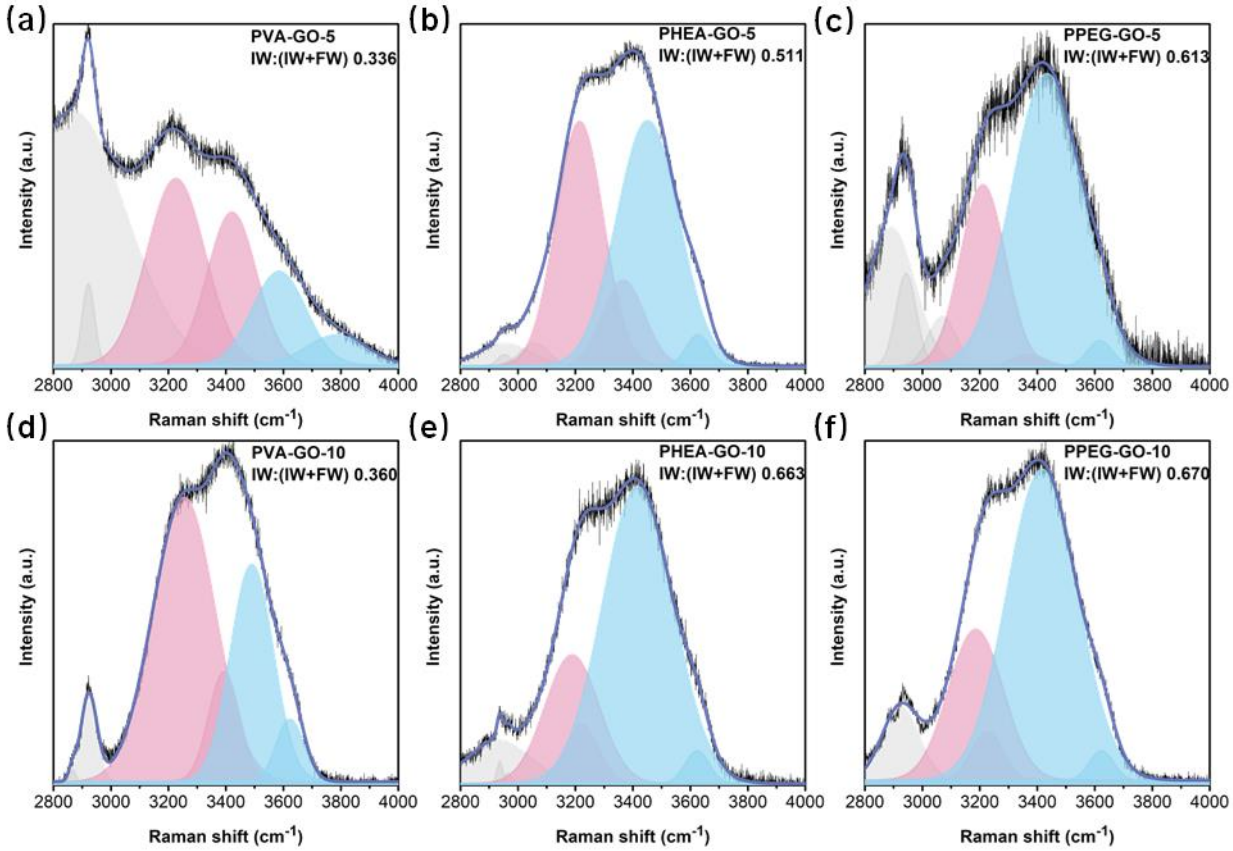

Figure 4. Fitting curves in the O-H stretching energy region for (a) PVA-GO-5, (b) PHEA-GO-5, (c) PPEG-GO-5, (d) PVA-GO-10, (e) PHEA-GO-10 and (f) PPEG-GO-10 in Raman spectrum. The pink peaks and light blue peaks represent free water and intermediate water, respectively.

(IW)/(IW+FW) ratio of 0.36:1, 0.663:1 and 0.67:1 for PVA-GO-10, PHEA-GO-10 and PPEG-GO-10, respectively. This result also suggests that different hydrophilic functional groups, such as primary or secondary hydroxyl groups and C-O-C ether groups, would have different activation ability to promote the generation of IW water. Unfortunately, it seems that previous studies have overlooked the impact of hydrophilic functional groups in the water managements.

With rapid water replenishment capability and higher IW content, the cryogel-based SVGs are expected to display better solar vapor generation performance, which were determined by using a homemade setup under one sun irradiation as shown in Figure 5a. The gel was fixed in the middle of the expanded polyethylene (EPE) foam to ensure that the SVG can float on water surface, and paraffin film was used to seal any tiny gaps between the EPE foam and the container wall to prevent the potential bulk water evaporation. A balance was used to record the mass change of the container as a function of irradiation time and a thick EPE foam was also placed under the container to prevent potential heat transfer from the balance to the container. We took infrared images (Figure S3) to record the temperatures of the evaporation surface and the bulk water during the solar vapor generation process (Figure 5b). After 20 min irradiation, all SVG surfaces could be heated to a dynamic equilibrium temperature of 37-40 °C, which is higher than that of bulk water (*ca.* 30 °C), indicating that the converted energy was confined on the surface of the gels. We then recorded the mass changes of the bulk water with SVGs applied as a function of time. Of particular note, all the mass loss *vs.* time curves shown in Figure 5c have been calibrated by subtracting dark evaporation values and were estimated by the slopes of the mass loss−time curve through a linear fitting. All of the SVGs demonstrated substantially faster vapor generation rate than

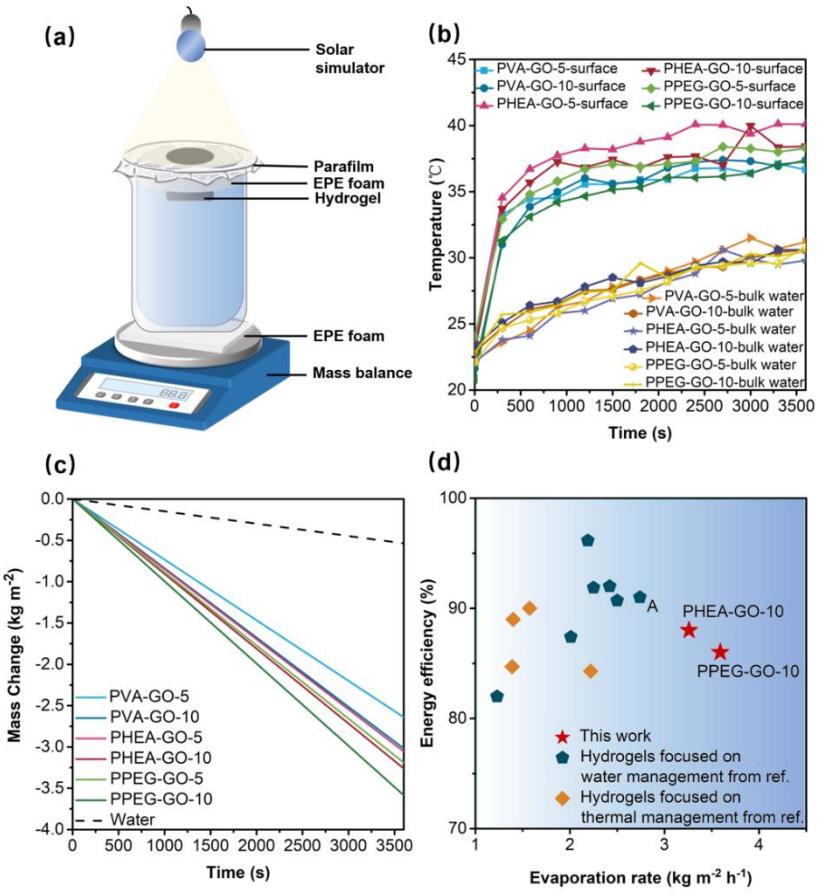

Figure 5. (a) The setup for the solar vapor generation test. (b) The temperatures of the gel surface and bulk water during the one hour of solar vapor generation test under 1 sun. (c) Water mass changes of PVA hydrogels, PHEA cryogels, PPEG cryogels and the pure water without any gels during the solar vapor generation test under 1 sun irritation. All the data have been calibrated with dark evaporation data and were estimated by the slopes of the mass−time curve via linear fitting. (d) Comparison of the evaporation rate and energy efficiency to the hydrogel SVGs in previous works with similar testing setup (The testing gel is fixed in the middle of a floating foam and the gel itself can directly contact the bulk water. Notely, the gel surface should not be much high above the foam surface). Detailed data are listed in Table S3.

that of pure water (without gels). Among them, cryogels PPEG-GO-10 and PHEA-GO-10 showed excellent solar vapor generation performance with an evaporation rate of 3.59 and 3.26 kg $m^{-2}h^{-1}$ respectively, higher than that the PVA-GO-10 (3.02 kg $m^{-2}h^{-1}$). It is worth noting that the excessive water in PHEA-GO-5 resulted in heat loss at the evaporating interface.[27, 55] As a result, even with a higher intermediate water content, the evaporation rate of PHEA-GO-5 is still similar to that of PVA-GO-10. Additionally, the evaporation rate of PPEG-GO-10-LN is lower than that of PPEG-GO-10 cryogel evaporator (Figure S2c).

The equivalent evaporation enthalpies (Table S2) in this study were determined by DSC-TGA measurements (Figure S4), and the calculated energy conversion efficiencies are presented in Figure S5. The equivalent evaporation enthalpy of PVA-GO-10, PHEA-GO-10 and PPEG-GO-10 was 1172.2 J g^{-1}, 972.74 J g^{-1} and 861.5 J g^{-1}, respectively, which was in good agreement with the corresponding trend of intermediate water content and evaporation rate. The P-GO-5 SVGs with lower polymer contents but higher saturated water contents showed lower evaporation rates, because of their relative lower intermediate water contents. Furthermore, the solar-thermalenergy efficiency were calculated by equation (2):

$$\eta = \frac{\dot{m} \times h_v}{C_{opt} \times P_0} \quad \text{Eq. (2)}$$

where $\dot{m}$, h_v, C_{opt} and P_0 refer to the evaporation mass flux, the equivalent evaporation enthalpy of the water in the gel, the optical concentration, and the solar irradiation power (1 kW m^{-2}), respectively. Although all the gel SVGs only contain < 2wt% of GO, their photo-thermal energy conversion efficiencies were all above 85%, indicating efficient utilization of solar energy.

In previous literature, there have been several gel-based SVGs showing better performance such as 3D evaporator[56] in which the side walls also contribute to the evaporation. For fair comparison, we only collected the evaporation rate and energy efficiency data of the evaporators using similar SVG testing setup, and the detailed comparison is shown in Figure 5d and Table S3. With this setup, all the reported SVGs have good energy efficiency of >80 %.

We found that the evaporation rates of SVG systems is not positively correlated with energy efficiency, suggesting that low water-equivalent evaporation enthalpies and fast rehydration rate determine the water evaporation rate of SVG compared with high energy efficiency. Specifically, the hydrogel-based SVGs that focused on water management (blue pentagons) mostly have higher evaporation rate than those that focused on thermal management (orange diamonds). For example, the SVG point A presented [57] used the unidirectional freezing method to construct vertically rapid water transport channels, and it has much higher evaporation rate than other gels mainly focused on thermal management. Moreover, instead of using complex fabrication method (i.e. 3D printing), the SVG PPEG-GO-10 reported in our work, with interconnected rapid water transport channels and high IW content, greatly surpassed all other SVG systems including point A in term of performance.

With promising cryogel SVGs in hand, we then explored their desalination performance in practical applications. We have repeatedly tested the evaporation performance of PHEA-GO-10 (Figure 6a) and PPEG-GO-10 (Figure 6b) using seawater (Darling Harbour, Sydney, Australia; E151.20°, S33.87°). We conducted three-hours continuous seawater solar vapor generation test every day. During fourteen repeats, both PHEA-GO-10 and PPEG-GO-10 SVGs presented stable evaporation rates around 3.3 kg m^{-2} h^{-1} and 3.6 kg m^{-2} h^{-1} respectively under one sun irradiation. After each desalination process, no significant salt accumulation was observed on the surfaces of the SVG gels, suggesting good salt resistance (Figure S6). This might arise from the high water content and rapid water replenishment of cryogel networks, which could hinder the rapid concentration reduction at the evaporation surface and the super-saturation of salt solutions.[53] To collect the condensed water, the SVGs were placed ina sealed jar with glass cover and the condensed water at the bottom as well as on the wall of the container was collected for further analysis (Figure 6c). The ICP-MS measurements were performed to determine the salt concentrations of the seawater and the collected water, and the results were shown in Figures 6d-6e. We found that the concentrations of the primary ions (Na^+, Mg^{2+}, K^+ and Ca^{2+}) in the seawater were significantly reduced by 2-5 orders of magnitude after SVG-based

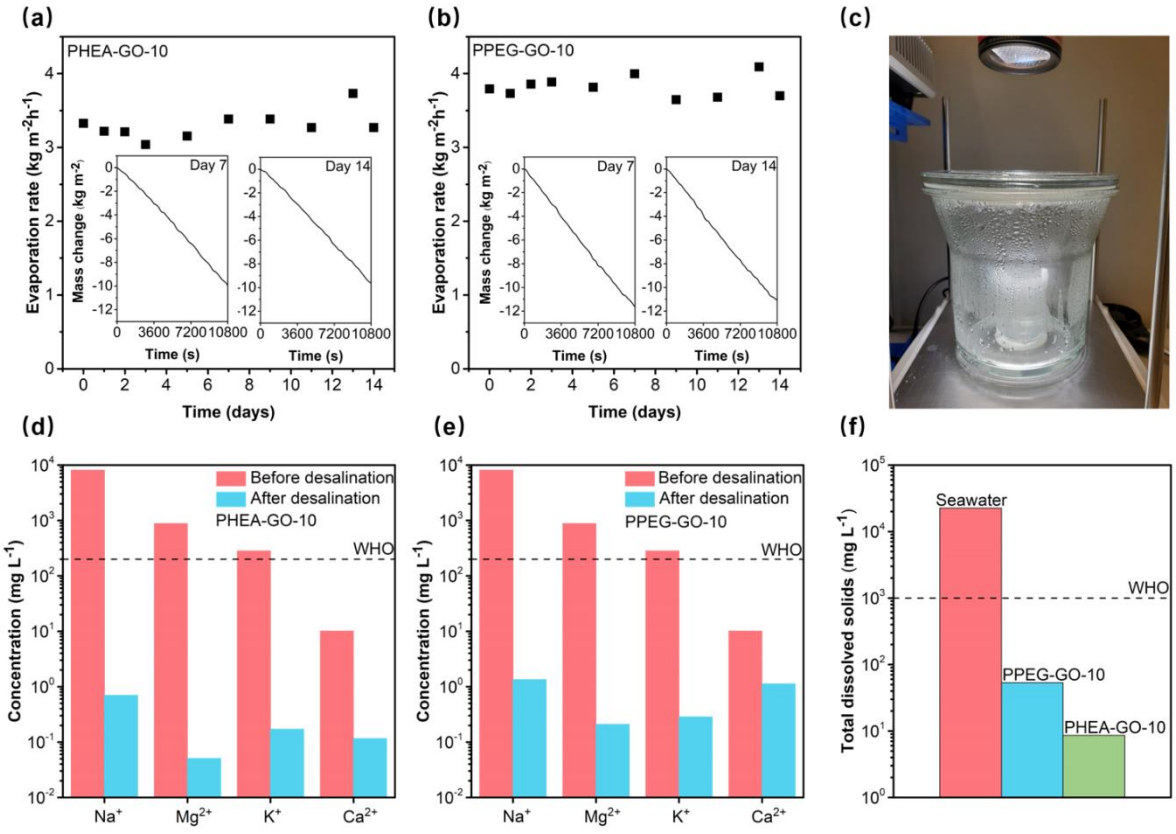

Figure 6. Desalination performance of the cryogels. Evaporation rates of (a) PHEA-GO-10 and (b) PPEG-GO-10 immersed in real seawater for half a month. Insets: solar vapor generation performance after seven and fourteen days of exposure to seawater. (c) The setup for desalination and condensed water collection. Four major ions concentrations measured in real seawater both before and after solar desalination via (d) PHEA-GO-10 and (e) PPEG-GO-10. (f) Total dissolved solids of the seawater and the desalinated water of PPEG-GO-10 and PHEA-GO-10.

desalination process. The seawater we used has a total dissolved solids (TDS) of 22,500 mg L^{-1}, and the TDS of the condensed water was 8.59 mg L^{-1} and 53.2 mg L^{-1} for PHEA-GO-10 and PPEG-GO-10 SVGs (Figure 6f). Notably, the salt concentrations in the produced water are lower than the World Health Organization (WHO) drinking water standards.[58-60] In all, the cryogel SVGs exhibit high salt resistance and highly stable performance in long-time solar desalination process.

Conclusion

In this study, we developed novel cryogel-based SVG materials via facile freeze-thaw method for solar driven desalination applications, and fairly compared their properties and performance with conventional hydrogel-based SVG systems. We found that the key for successful constructing macroporous water channels in cryogels is the selection of polymer precursors with T_gs below the freezing temperatures. In addition, the chemical structures of different hydrophilic groups also play an important role in promoting the IW water generation, thereby reducing the overall evaporation enthalpy. The resultant PHEA- and PPEG-based SVGs show rapid water replenishment ability and possess high intermediate water content, achieving easier water evaporation compared to conventional hydrogels. The cryogel SVGs also display excellent durability and desalination competence, which makes them promising for future practical desalination applications.

Experimental section

Materials

Chemicals including graphene oxide (GO powder, 15-20 nanosheets, 4-10% edge-oxidized), PVA (MW 89000-98000), glutaraldehyde (GA) solution (25 wt% in DI water), hydrochloric acid (32 wt% in DI

Please do not adjust margins

water), 2-hydroxyethyl acrylate (HEA, 96 wt% in DI water), *N,N'*-methylenebis(acrylamide) (MBI), *N,N,N',N'*-tetramethyl-ethylenediamine (TEMED), ammonium persulfate (APS), poly(ethylene glycol) diacrylate (PEGDA, average M_n = 575 g mol^{-1}) were all purchased from Sigma-Aldrich and used without further purification.

Synthesis of PVA-based hydrogels

Typically, PVA (100 mg, MW = 89,000-98,000 g mol^{-1}) was added into a GO solution (1.9 mL, 1 mg/mL in DI water) and heated under 80 ℃ for 5 hours (A). Then, glutaraldehyde solution (40 μL, 25 wt% in DI water) and DI water (41 uL) were added in and mixed together by sonication. Next, HCl (50 μL, 32 wt% in DI water) were added to trigger the gelation. The obtained gel was frozen overnight at -18 ℃, thawed in DI water overnight, and washed with DI water three times to obtain a pure PVA-GO-5 hydrogel. PVA-GO-10 was prepared in a similar manner, merely changing the amount of the PVA and GA used. All the hydrogels were freeze-dried before characterization, and saturated in DI water or seawater before Solar vapor generation tests.

Synthesis of PHEA-based cryogels

Typically, 2-hydroxyethyl acrylate (HEA, 87.16 mg, 96 wt% in DI water), *N,N'*-methylenebis(acrylamide) (12.83 mg), *N,N,N',N'*-tetramethyl-ethylenediamine (TEMED, 10 μL) and GO solution (1.9 mL, 1 mg/mL in DI water) were mixed together by sociation. Then an ammonium persulfate solution (APS, 0.1 mL, 0.03 g/mL in DI water) was added in and mixed together to trigger the gelation. The obtained gel was frozen overnight at -18 ℃, thawed in DI water overnight, and washed with DI water three times to obtain a pure PHEA-GO-5 cryogel. PHEA-GO-10 was prepared in a similar manner, merely changing the amount of the HEA and MBI used. All the cryogels were freeze-dried before characterization, and saturated in DI water or seawater before solar vapor generation tests.

Synthesis of PPEG-based cryogels

Typically, poly(ethylene glycol) diacrylate (PEGDA, 100 mg, average Mn 575 g mol^{-1}), *N,N,N',N'*-tetramethyl-ethylenediamine (TEMED, 10 μL) and GO solution (1.9 mL, 1 mg/mL in DI water) were mixed together by sociation. Then an ammonium persulfate solution (APS, 0.1 mL, 0.03 g/mL in DI water) was added in and mixed together to trigger the gelation. The obtained gel was frozen overnight at -18 ℃, thawed in DI water overnight, and washed with DI water three times to obtain a pure PPEG-GO-5 cryogel. PPEG-GO-10 was prepared in a similar manner, merely changing the amount of the PEG used. All the cryogels were freeze-dried before characterization, and saturated in DI water or seawater before Solar vapor generation tests.

Solar vapor generation tests

A solar simulator (NBeT HSX-F3000 xenon light source) was used to produce 1 sun irradiation (1 kW/m^2) and the solar irradiance on the gel surface was measured by a compact power and energy meter console (PM100D, Thorlabs, Germany) with a thermal power sensor (S405C, Thorlabs, Germany). The gel for testing was fixed in a EPE foam, and floated on the top of a beaker full of DI water or seawater. A Paraffin film was used to cover a few tiny spaces between the EPE foam and the beaker to prevent the potential impact of bulk water evaporation. The mass changes during the SVG process were recorded by an electronic mass balance (OHAUS Pioneer IC-PX 124) every 4 minutes. There was also a EPE foam between the beaker and mass balance for thermal insulation. The evaporation rates were estimated by the slopes of the mass−time curve via linear fitting. The temperatures of the hydrogel surface and the bulk water during the solar vapor generation tests were collected every 5 minutes by a Fluke PTi120 pocket thermal imager.

Characterizations

The internal morphology of the hydrogels was observed using a Zeiss scanning electron microscope (SEM) (10–30 kV). Fourier transform infrared spectroscopy (FT-IR) was obtained with Shimadzu MIRacle 10 FT-IR. UV-visible-NIR absorbance spectra was collected using a Shimadzu 1700 UV–Vis-NIR spectrophotometer operating in the wavelength range 300-2500 nm. Raman spectrum was collected by a Renishaw Raman spectroscopy. The heat change of gels from room temperature to 200 ℃ was monitored using a Q600 SDT Thermal Analyzer (DSC-TGA) at a heating rate of 10 ℃ min^{-1}. The ion concentrations in the desalinated water and seawater were analyzed with Agilent 7900 ICP-MS. The total dissolved solids (TDS) of the desalinated water and seawater were tested by a HQ40D Portable Multi Meter.

Conflicts of interest

The authors declare no competing financial interest.

Acknowledgements

Qiang Fu acknowledges the Australian Research Council under the Future Fellowship (FT180100312). Shudi Mao acknowledges support from the China Scholarship Council (CSC) Scholarship (202006140015).

References

1. D. N. Chakkaravarthy, *International Journal of Agriculture Environment and Biotechnology*, 2019, **12**, 187-193.
2. A. Panagopoulos, K.-J. Haralambous and M. Loizidou, *Science of The Total Environment*, 2019, **693**, 133545.
3. R. Semiat, *Environmental science & technology*, 2008, **42**, 8193-8201.
4. A. D. Khawaji, I. K. Kutubkhanah and J.-M. Wie, *Desalination*, 2008, **221**, 47-69.
5. F. A. AlMarzooqi, A. A. Al Ghaferi, I. Saadat and N. Hilal, *Desalination*, 2014, **342**, 3-15.
6. A. Al-Karaghouli and L. L. Kazmerski, *Renewable Sustainable Energy Reviews*, 2013, **24**, 343-356.
7. S. Al-Amshawee, M. Y. B. M. Yunus, A. A. M. Azoddein, D. G. Hassell, I. H. Dakhil and H. A. Hasan, *Chemical Engineering Journal*, 2020, **380**.
8. C. Y. Tang, Z. Yang, H. Guo, J. J. Wen, L. D. Nghiem and E. Cornelissen, *Environ Sci Technol*, 2018, **52**, 10215-10223.
9. Z. Deng, J. Zhou, L. Miao, C. Liu, Y. Peng, L. Sun and S. Tanemura, *Journal of Materials Chemistry A*, 2017, **5**, 7691-7709.

Please do not adjust margins

Please do not adjust margins

10. O. Neumann, A. S. Urban, J. Day, S. Lal, P. Nordlander and N. Halas, *ACS nano*, 2013, **7**, 42-49.
11. S. Ma, C. P. Chiu, Y. Zhu, C. Y. Tang, H. Long, W. Qarony, X. Zhao, X. Zhang, W. H. Lo and Y. H. Tsang, *Applied energy*, 2017, **206**, 63-69.
12. S. Mao, M. Johir, C. Onggowarsito, A. Feng, L. Nghiem and Q. Fu, *Materials Advances*, 2022, **3**, 1322-1340.
13. F. Zhao, Y. Guo, X. Zhou, W. Shi and G. Yu, *Nature Reviews Materials*, 2020, **5**, 388-401.
14. X. Zhou, Y. Guo, F. Zhao and G. Yu, *Acc Chem Res*, 2019, **52**, 3244-3253.
15. T. Yang, H. Lin, K.-T. Lin and B. Jia, *Sustainable materials technologies*, 2020, **25**, e00182.
16. Y. Wang, J. Zhang, W. Liang, H. Yang, T. Guan, B. Zhao, Y. Sun, L. Chi and L. Jiang, *CCS Chemistry*, 2021, 1-39.
17. I. Ibrahim, D. H. Seo, A. M. McDonagh, H. K. Shon and L. Tijing, *Desalination*, 2021, **500**, 114853.
18. Y. Guo, F. Zhao, X. Zhou, Z. Chen and G. Yu, *Nano letters*, 2019, **19**, 2530-2536.
19. F. Yang, J. X. Chen, Z. Y. Ye, D. W. Ding, N. V. Myung and Y. D. Yin, *Advanced Functional Materials*, 2021, **31**, 9.
20. Y. Lu, D. Fan, Y. Wang, H. Xu, C. Lu and X. Yang, *ACS nano*, 2021, **15**, 10366–10376.
21. Y. Guo, H. Lu, F. Zhao, X. Zhou, W. Shi and G. Yu, *Adv Mater*, 2020, **32**, 1907061.
22. H. Zhou, C. Xue, Q. Chang, J. Yang and S. Hu, *Chemical Engineering Journal*, 2021, **421**, 129822.
23. C. Tian, C. Li, D. Chen, Y. Li, L. Xing, X. Tian, Y. Cao, W. Huang, Z. Liu and Y. Shen, *Journal of Materials Chemistry A*, 2021, **9**, 15462-15471.
24. Z. Liu, R.-K. Qing, A.-Q. Xie, H. Liu, L. Zhu and S. Chen, *ACS Applied Materials and Interfaces*, 2021, **13**, 18829-18837.
25. B. Wen, X. Zhang, Y. Yan, Y. Huang, S. Lin, Y. Zhu, Z. Wang, B. Zhou, S. Yang and J. Liu, *Desalination*, 2021, **516**, 115228.
26. M. Tan, J. Wang, W. Song, J. Fang and X. Zhang, *Journal of Materials Chemistry A*, 2019, **7**, 1244-1251.
27. X. Zhang, Y. Peng, L. Shi and R. Ran, *ACS Sustainable Chemistry & Engineering*, 2020, **8**, 18114-18125.
28. X. Wu, Y. Wang, P. Wu, J. Zhao, Y. Lu, X. Yang and H. Xu, *Advanced Functional Materials*, 2021, **31**, 2102618.
29. T. Li, Q. Fang, J. Wang, H. Lin, Q. Han, P. Wang and F. Liu, *Journal of Materials Chemistry A*, 2021, **9**, 390-399.
30. J. Chen, M. Lee, Y. Qiu, C. Wu, B. Li and Y. Yin, *SmartMat*, 2022, DOI: 10.1002/smm2.1140.
31. Y. Guo, X. Zhou, F. Zhao, J. Bae, B. Rosenberger and G. Yu, *ACS Nano*, 2019, **13**, 7913-7919.
32. F. Zhao, X. Zhou, Y. Shi, X. Qian, M. Alexander, X. Zhao, S. Mendez, R. Yang, L. Qu and G. Yu, *Nat Nanotechnol*, 2018, **13**, 489-495.
33. H. Wang, R. Zhang, D. Yuan, S. Xu and L. Wang, *Advanced Functional Materials*, 2020, **30**, 2003995.
34. D. Lapotko, *Optics express*, 2009, **17**, 2538-2556.
35. Z. Yu and P. Wu, *Advanced Materials Technologies*, 2020, **5**, 2000065.
36. J. X. He, Y. K. Fan, C. H. Xiao, F. Liu, H. X. Sun, Z. Q. Zhu, W. D. Liang and A. Li, *Compos. Sci. Technol.*, 2021, **204**, 9.
37. Z. Wang, Z. Zhan, L. Chen, G. Duan, P. Cheng, H. Kong, Y. Chen and H. Duan, *Solar RRL*, 2022, **6**, 2101063.
38. X. Zhou, Y. Guo, F. Zhao, W. Shi and G. Yu, *Adv Mater*, 2020, **32**, 2007012.
39. A. Baimenov, D. A. Berillo, S. G. Poulopoulos and V. J. Inglezakis, *Adv Colloid Interface Sci*, 2020, **276**, 102088.
40. V. M. Gun'ko, I. N. Savina and S. V. Mikhalovsky, *Adv Colloid Interface Sci*, 2013, **187-188**, 1-46.
41. V. I. Lozinsky, *Russian Chemical Reviews*, 2002, **71**, 489-511.
42. V. I. Lozinsky, in *Polymeric Cryogels*, ed. O. Okay, Springer, Cham, 2014, vol. 263, ch. Chapter 1, pp. 1-48.
43. V. I. Lozinsky and O. Okay, in *Polymeric Cryogels*, ed. O. Okay, Springer, Cham, 2014, vol. 263, ch. Chapter 2, pp. 49-101.
44. O. Okay and V. I. Lozinsky, in *Polymeric Cryogels*, ed. O. Okay, Springer, Cham, 2014, vol. 263, ch. Chapter 3, pp. 103-157.
45. S. Dech, V. Wruk, C. P. Fik and J. C. Tiller, *Polymer*, 2012, **53**, 701-707.
46. N. S. Vrandečić, M. Erceg, M. Jakić and I. Klarić, *Thermochimica Acta*, 2010, **498**, 71-80.
47. A. Southan, E. Hoch, V. Schönhaar, K. Borchers, C. Schuh, M. Müller, M. Bach and G. E. Tovar, *Polymer Chemistry*, 2014, **5**, 5350-5359.
48. M. Koosha, H. Mirzadeh, M. A. Shokrgozar and M. Farokhi, *RSC advances*, 2015, **5**, 10479-10487.
49. A. Shrivastava, in *Introduction to Plastics Engineering*, ed. A. Shrivastava, William Andrew Publishing, 2018, DOI: 10.1016/B978-0-323-39500-7.00001-0, pp. 1-16.
50. H. Zhang, L. Li, N. He, H. Wang, B. Wang, T. Dong, B. Jiang and D. Tang, *EcoMat*, 2022, **4**.
51. X. Zhou, F. Zhao, Y. Guo, Y. Zhang and G. Yu, *Energy & Environmental Science*, 2018, **11**, 1985-1992.
52. C.-S. Hu, H.-J. Li, J.-Y. Wang, A. Haleem, X.-C. Li, M. Siddiq and W.-D. He, *ACS Applied Energy Materials*, 2019, **2**, 7554-7563.
53. S.-L. Loo, L. Vásquez, M. Zahid, F. Costantino, A. Athanassiou and D. Fragouli, *ACS Applied Materials and Interfaces*, 2021, **13**, 30542–30555.
54. J.-Y. Wang, X.-X. Guo, J. Chen, S.-C. Hou, H.-J. Li, A. Haleem, S.-Q. Chen and W.-D. He, *Materials Advances*, 2021, **2**, 3088-3098.
55. M. Yang, H. Luo, W. Zou, Y. Liu, J. Xu, J. Guo, J. Xu and N. Zhao, *ACS Appl Mater Interfaces*, 2022, **14**, 24766-24774.
56. Y. Xu, J. Xu, J. Zhang, X. Li, B. Fu, C. Song, W. Shang, P. Tao and T. Deng, *Nano Energy*, 2022, **93**.
57. Y. Tian, X. Liu, S. Xu, J. Li, A. Caratenuto, Y. Mu, Z. Wang, F. Chen, R. Yang, J. Liu, M. L. Minus and Y. Zheng, *Desalination*, 2022, **523**, 115449.
58. W. H. Organization, *Potassium in drinking-water: background document for development of WHO guidelines for drinking-water quality*, World Health Organization, 2009.
59. W. H. Organization, *Calcium and magnesium in drinking water: public health significance*, World Health Organization, 2009.
60. G. WHO, *World health organization*, 2011, **216**, 303-304.

This journal is © The Royal Society of Chemistry 20xx

Please do not adjust margins